Measuring Specific Absorption Rate of Antennas Placed Near Human Body

Samah Beg*, Miguel Gonzalez†, Dr. Christopher Davis‡, and John Rzasa§

MERIT BIEN 2010, University of Maryland, College Park

* George Washington University, sbeg@gwmail.gwu.edu
† University of Pennsylvania, miguelg@seas.upenn.edu
‡ University of Maryland, davis@umd.edu
§ University of Maryland, rzasaman@umd.edu

***Abstract*—The FCC has set exposure limits on the amount of radiation that can be emitted from wireless devices and absorbed by the human body. This is determined by measuring the amount of energy absorbed by the body, or the Specific Absorption Rate (SAR). Current methods for measuring the SAR from cell phones placed near the human body are somewhat inaccurate and slow, the equipment involved is large and expensive, and there is room for improvement. The testing method we are studying incorporates a base station emulator that calls a phone whose radiation is absorbed by a model of the human body consisting of a saline solution inside a glass structure. By projecting a set of lasers through the structure and measuring their deflection due to a change in index of refraction, one can measure the rate of temperature rise of the model which determines the amount of energy absorbed. To make this method reliable the lasers used must point accurately through the absorbing medium at lateral effect photodiodes. The principle goal of our project is to study and improve the stability of this laser pointing.**

***Index Terms*—Specific Absorption Rate, Pointing Stability, Lateral Effect Photodiode**

I. Introduction

The advancement of technological design and comprehension has given todays society the ability to conceive and perform upon ideas once considered impossible; with a simple push of a button or twist of a knob, mankind can wield the power to communicate globally, maneuver a motor craft, or even destroy an entire city. Every technological aspect has certain underlying and often misunderstood health and safety principles associated with it that vary in severity. For instance, there are well-known risks associated with firing a nuclear warhead; the price of imperialistic supremacy is paid for with the lives of millions and the biological deterioration of the land in which the bomb was detonated. Unfortunately, not every situation is so simple to diagnose as in the case of a nuclear holocaust, thus creating the impetus for further scientific research into new and existing technology and how it interacts within our environment. One field of active research discussed herein is that of telecommunications.

Developments within the field of telecommunications have been crucial in establishing diplomatic relationships, global enterprises, and the way we perceive our society. What started out as simple smoke signals between neighboring villages has erupted into a full gamut of communication and networking protocols that tie our world together. One device in particular that has been monumental in breaking the tether of conventional fixed point communication by allowing people to roam while connecting to their outside lives is the cellular phone.

The operation of a cellular phone is based on two-way radio communication established over a network of cell sites. Each cell site is located at a base station consisting of a high-power antenna that both transmits and receives incoming calls between phone and station, establishing a handoff configuration that covers a broad service area. For the base station to establish a clear connection to phones within its far-field distance, RF signals comprised of frequencies within, for example, the standard GSM-900 or GSM-1800 MHz bands are radiated through the air to the receiving antenna. This implies that RF radiation is present at all times within the environment that the phone is operated in, including the human head. These allegations have caused a media-based hysteria linking long-term cell phone usage to infertility, nerve cell damage, and even cancer. Several studies have been conducted that provide both support [1] and refutation [2] for this claim, but there is no conclusive data to prove health risk.

One method for testing the effects of RF radiation on the body is by measuring the Specific Absorption Rate (SAR), or rate at which RF energy is absorbed by the body. In order to ensure that transmitters do not expose the public to unnecessary risk, the Federal Communications Commission (FCC) has capped the maximum SAR rating for wireless devices at 1.6 W/kg averaged over any cubic centimeter of tissue anywhere in the body [3]. Current systems are in place to measure the SAR with a phone in the vicinity of a phantom head; however, all available tests are slow, expensive, and unreliable. This paper proposes improvements upon a novel test set-up for measuring the spatial distribution of the rate of temperature rise within the phantom. Several lasers pass through the phantom and are deflected by the temperature gradients produced by the energy absorption; these deflections can then be measured and based upon a change in index of refraction of the media within the phantom, the SAR can be

calculated, providing a inexpensive and rapid system for future testing.

II. Theoretical Framework

A. Specific Absorption Rate

The SAR is defined as the time derivative of the differential energy (dW) either absorbed or dissipated in a differential mass (dm) within a differential volume (dV) of known density (ρ), or the rate at which energy is absorbed by the human body when exposed to RF electromagnetic fields as expressed by:

$$SAR = \frac{d}{dt}\frac{dW}{dm} = \frac{d}{dt}\frac{dW}{\rho dV} \tag{1}$$

Measured in units of Watts per kilogram (W/kg), the SAR reading is an averaged value over a sampling of tissue, usually 1 or 10 cm^3, but can be extended to a measurement over the entire body, and is calculated by measuring the slope of the temperature gradients in that region. More commonly, commercial SAR testing of RF devices is done using spatial measurements of electric field strength given by:

$$SAR = \int_V \frac{\sigma(r)\,|E(r)|^2}{\rho(r)} dr \tag{2}$$

where σ is the conductivity of the tissue (S/m), ρ is the mass density of the tissue (kg/m^3), and E is the rms value of the electric field (V/m).

In an attempt to regulate public safety associated with commerce, various governments in Europe and here in America have set safety limits for exposure to RF devices including, but not limited to, fixed or mobile transmitting devices that operate in the Cellular Radiotelephone, Personal Communications (PCS), and Wireless Medical Telemetry Service (WMTS) sections under FCC regulation [4]. SAR measurements on models of the human body are used to verify adherence to these regulations as they are noninvasive, and devices for making such measurements are currently in use, although there is currently no standard method specified by the FCC.

B. Photothermal Deflection

The physical principle under which the deflection of the laser beam is to occur is known as Photothermal Deflection (PTD), or more commonly referred to as the mirage effect. When the RF radiation is present within the phantom, there is a time and space dependent temperature gradient ∇T present in the stimulant fluid that is a maximum at the point of contact with the wireless device and falls off as one goes deeper into the tank or away from the point of contact, or as the device is removed and the heat is allowed to dissipate into the surround media.

The temperature gradient produced causes changes in the index of refraction n_T of the stimulant fluid, given by:

$$n_T = 1 + \frac{n_o - 1}{1 + \alpha T} \tag{3}$$

where n_o is the index of refraction at 0° C, α is a function of wavelength, and T is the temperature at a given point in space. It is evident from this equation that whever the temperature rises the most, the refractive index will be at a minimum. As the laser passes through the heated areas of the stimulant, the direction of the beam is bent proportionally to the value of α, which is usually very small and roughly constant. The induced refractive index gradient causes the finite thickness of the laser to split in two paths, with the upper part of the beam traveling at a different velocity (v_U) than the lower part (v_L) [5]. The main portion of the beam will then tend to travel along the path which reduces the amount of time it takes to reach its target, as opposed to the shortest geometric distance.

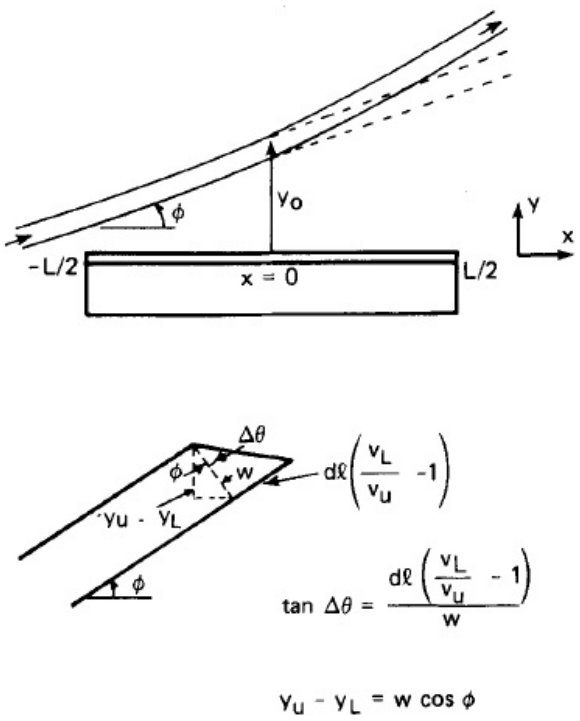

Fig. 1. Beam Deflection due to Temperature and Refractive Index Gradients [5]

Following the analysis of [5], the deflection of the beam, shown in Figure 1, is roughly linear and can be seen as a change in angular position along the differential path difference (dl) between the parts of the beam given by:

$$\triangle = dl(\frac{v_U}{v_L} - 1) \tag{4}$$

If a positive angular change is considered, it follows that:

$$d\theta = \tan(d\theta) = \frac{\triangle}{w} = \frac{(\frac{v_U}{v_L} - 1)dl}{w} \tag{5}$$

where w is the width of the traversing beam. Since this value is very small, one can approximate the difference in refractive indicies between the two parts of the beam as:

$$n_U = n_L + \frac{dn}{dy}(y_U - y_L) \tag{6}$$

where y_U and y_L are the distances of the upper and lower parts of the beam above the surface of the stimulant aong the

dl. Give that the difference between y_u and y_L is negligible, one can replace either of the above by $\text{wcos}(\phi)$ and $\text{dlcos}(\phi)$ by dx where ϕ is the incident angle of the light (see Figure 1). This results in a simplified expression given by;

$$d\theta = \frac{1}{n_L}\frac{dn}{dy}dx \approx \frac{1}{n}\frac{dn}{dy}dx \tag{7}$$

Integrating over the length of the surface of propagation, the total deflection of the laser beam is:

$$\theta = \int_{\frac{-L}{2}}^{\frac{L}{2}} \frac{1}{n}\frac{dn}{dy}dx \tag{8}$$

The rate of change in the index of refraction can be tied back to the rate of change of temperature using the chain rule:

$$\frac{dn}{dy} = \frac{dn}{dT}\frac{dT}{dy} \tag{9}$$

Substiuting the relationship between index of refraction and temperature as modeled in Equation 3, the result is:

$$\frac{dn}{dy} = -\alpha\frac{n_o - 1}{(1+\alpha T)^2}\frac{dT}{dy} \tag{10}$$

Thus given a known temperature distribution and integrating over the length of propagation, the total deflection of the beam can be calculated as:

$$\theta = -\alpha(n_o - 1)\int_{\frac{-L}{2}}^{\frac{L}{2}} \frac{dT}{dy}dx \tag{11}$$

III. Motivation

A common existing method of cell phone SAR testing is shown in Fig 2. The apparatus on the left consists of an automated mechanical arm with an attached probe at the end that extends into a phantom mold of a human head/torso. The mold is filled with a stimulant fluid that mimics the electrical properties of human flesh. Underneath the mold is a device that holds a cell phone in various positions while the probe measures the amount of energy absorbed when the phone is emitting a signal at its maximum power [6].

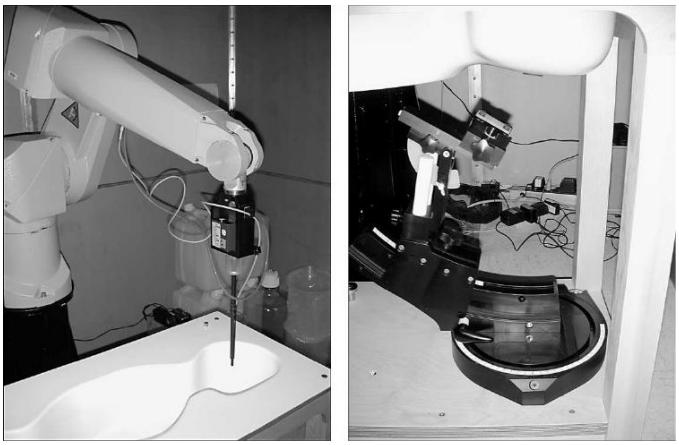

Fig. 2. FCC's Mobile Phone SAR Test Equipment [6]

Although used by many companies for wireless device testing, this apparatus is bulky, slow, costly, and varying in accuracy. Thus, designing a faster, cost-effective, and more accurate and compact system for measuring the SAR of wireless devices is a necessary goal in this current technological era; with new devices being designed and marketed so rapidly, cutting down on the time it takes to test each product for adherence to current FCC standards would be beneficial.

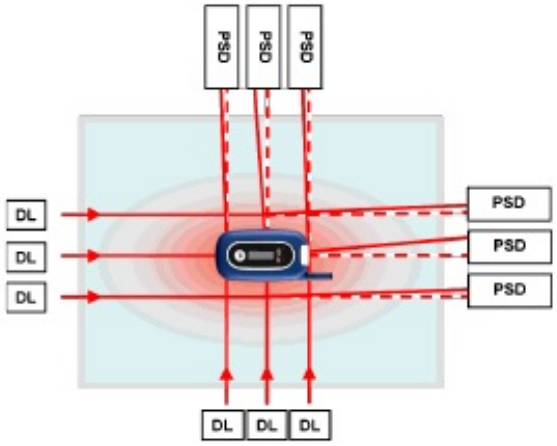

Fig. 3. Rapid Optical SAR Measuring Device [7]

Davis et al. have worked on a new prototype that will remedy all the hinderances caused by current testing methods. This design is based upon the principle of photothermal deflection in which rising temperature rates caused by RF absorption are used to measure the SAR of cellular phones and other wireless devices [7]. Their recent experimentation consisted of using a sealed glass tank filled with a saline stimulant that has a dielectric constant similar to that of human tissue. Six diode lasers, three on each of two sides of the tank, were mounted stably to an optical table and raised on a solid block in order to pass through the solution as close to the top of the tank as possible. Opposite to the lasers are six stably mounted position sensitive detectors (PSD), used to detect the position of the corresponding laser beams coming through the tank, as shown in Fig 3. The PSD outputs are amplified and measured through an analog-to-digital converter, which is interfaced with a PC for automated collection of position data with respect to time. To run the test, a cell phone is placed in the cradle above the tank and called by manually entering commands into a Willtek 4202S base station emulator that causes the phone to go from minimum to maximum power. The RF energy emitted by the cell phone during this call causes the solution in the tank to heat up, resulting in a change in the index of refraction of the solution closest to the antenna. This change is seen in the deflection of the laser beam passing through the solution. The motivation for our project stems from problems encountered with this setup, primarily with the thermal drift present at the laser output due to thermal conduction arising from human contract with the apparatus, laser instabilities, coupling lens imperfection, and nonideal environmental control.

IV. Contribution

The primary goal of this project is to characterize and improve the pointing stability of the lasers being used, as this was the main issue encountered with the previous experimental setup. Ideally, the laser beam through the final setup should be narrow, constant, and unwavering to yield the most accurate results. To achieve this, both the lasers and PSDs need to be stably mounted to a rigid surface in order to minimize unwanted Brownian motion inherent in the system due to fluctuations and interference from the surrounding environment.

A. Adjustments to Previous Design

A similar setup to that which was outlined previously is used in this project, with a few adjustments to the components being used. A single mode, 660 nm wavelength, fiber-pigtailed laser replaced the diode lasers. This single mode fiber is designed such that the light traversing through its inner core is guided due to the total internal reflections between its core and cladding and the output supports only single frequency propagation. The single mode fiber was chosen because of the tranverse intensity profile that is emitted from the tip of the fiber maintains a fixed Gaussian beam distribution regardlesss of how the light is inputted [8].

Furthermore, the Willtek 4202S base station emulator was interfaced with a PC via serial port in order to automate calls to the cell phone. Commands are sent to the Willtek machine through a LabView VI. The machine then executes the command and establishes a connection with the cell phone. This will be used in future work on this project.

B. Mounting of Components

In order to achieve a high degree of stability and reduce any mechanical vibration in the system, custom mounts of aluminum were made for each component. The FC connector of the pigtailed laser was mounted directly onto a three-axis stage to allow adjustability of the output beam; the microscope objective was attached to a solid block on an existing lens holder; and a block with an aperture for the pinhole. The pinhole was drilled into a thin sheet of metal which was placed over the larger aperture in the aluminum block, as opposed to drilling the pinhole directly through the block. This was done to prevent scattering of the beam inside the block. The PSD itself was soldered into a PC board that was screwed into its own block. All components were then mounted firmly to an optical table to increase stability of the overall system.

V. Methodology

The laser beam needed to be collimated and focused so that it would be sufficiently narrow in order to increase sensitivity to the RF absorption within the tank and take reliable measurements using the PSD. This was accomplished by placing a 3x microscope objective directly in front of the laser, followed by a 0.5 mm-diameter pinhole to narrow the beam onto the 10 mm x 2 mm surface of the PSD. A 12-inch glass cube was used to hold the saline solution, and a thin plastic tray was made to fit into the tank to rest on the surface of this solution, reducing any meniscus effects. This tank was placed between the pinhole and the PSD mount during the later stages of testing.

A LabVIEW virtual instrument (VI) is used for data collection throughout testing of the system. The VI would read in values from the PSD interfaced to a 16-bit A-D converter and record the results into a text file. The data from the PSD consisted of an output voltage that was proportional to the variation of the laser centroid incident upon the PSD. The relative position of the centroid (Y) can be calculated from a ratio of two currents using:

$$Y = \frac{Y_1 - Y_2}{Y_1 + Y_2} \frac{L}{2} \tag{12}$$

where Y_1 and Y_2 are the signals out of the anodes of the PSD and L is the length of the detector. The PSD was rated to output voltages from -10 to +10 V over the 10 mm surface, so to find the change in distance one can use the conversion factor that 1mV = 0.5 μmeters.

The pointing stability of the laser beam was tested in (A) open air, (B) with the unfilled tank, (C) with the plastic tray resting in the empty tank, and (D) with the stimulant-filled tank. For optimal performance of the PSD, the SUM output voltage of the PSD amplifying circuit should range from 5 V to 9 V. The various laser-driving current values were determined based on this range of the SUM output voltage. Each test was performed with the lights on and off, to account for any effect ambient light would have on PSD measurements.

A. Stability Through Air

For this portion of testing, the path of the laser beam emitted from the pinhole and incident upon the PSD was unobstructed. Measurements were taken at driving currents of 60 to 72 mA, in 3 mA increments.

B. Stability Through Unfilled Tank

The glass tank was placed between the pinhole and PSD, with the surface of the tank 0.5 in. away from both the pinhole and the surface of the PSD. Measurements were taken at driving currents of 67 to 85 mA, in 3 mA increments. The range of currents was increased to account for the decrease in the SUM output due to the placement of the tank, which decreased the intensity of the beam centroid on the PSD due to power loss from the refractive changes the beam experienced traveling through different media.

C. Stability Through Enclosed Tank

The plastic tray was then placed inside the empty tank, and measurements were taken at driving currents of 67 to 85 mA, in 3 mA increments. This data is useful to observe any effects convection air currents would have on the laser's trajectory and how isolation of the beam may improve its stability.

D. Stability Through Stimulant-Filled Tank

The tank was filled with water to a height approximately 4 inches from the base of the tank, and the plastic tray was placed on the surface of the water, in order to reduce the meniscus effect. Measurements of beam centroid position were taken for driving currents of 69 to 90 mA, in 3 mA increments.

VI. Results

A representative sampling of our results is shown in Figures 4 - 7 and analyzed more thoroughly in Tables I and II.

The data described in each chart shows the PSD output voltage drifting over time under each testing condition over a period of three minutes. The sample data was chosen to represent when the environment's lights were off so that the ambient light of the room would not create unwanted noise. The linear trend on each graph represents the beam's centroid with the y-intercept marking the starting position of the beam relative to the center of the PSD and the slope showing an overall increase or decrease in its relative position.

Table I represents averaged values for how the laser drifts from its starting position for each of the testing conditions. The average output voltage was calculated for each driving current and was subtracted from its starting value. These values were then averaged over all the runs for each condition to gauge which setup would cause the laser on to drift most. Table II shows the laser drift in micrometers, which was derived using the conversion factor from milliVolts to micrometers described above.

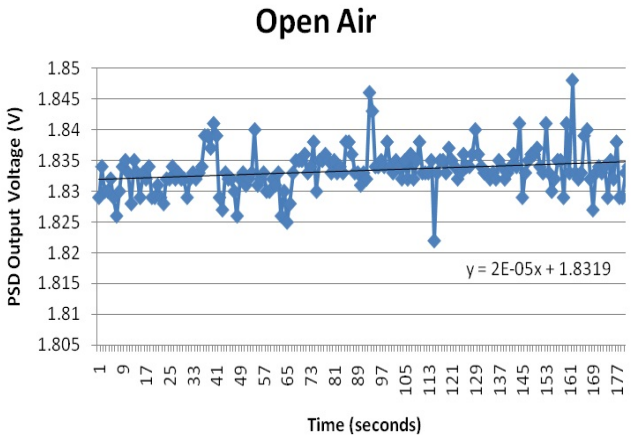

Fig. 4. Laser Drift vs. Time in Open Air Propagation

TABLE I
Laser Drift Output in milliVolts

	Open Air	Empty Tank	Enclosed Tank	Stimulant Tank
Ave. Drift	0.567	0.501	0.157	0.538
Std. Devation	6.325	2.149	2.181	5.285
Ave. Range	21.4	19.28	18.43	30.75
Std. Deviation	3.130	4.231	3.409	9.036

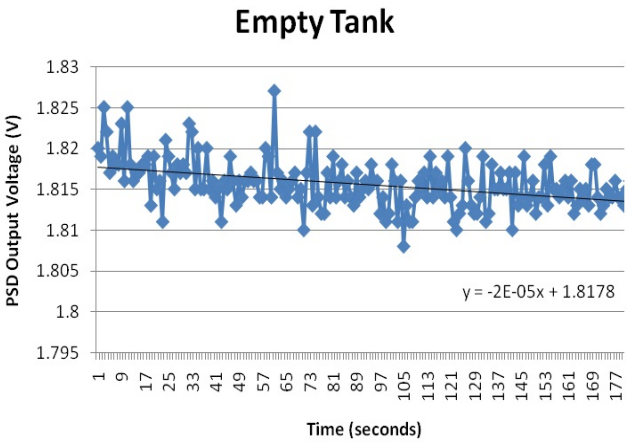

Fig. 5. Laser Drift vs. Time Through Empty Tank

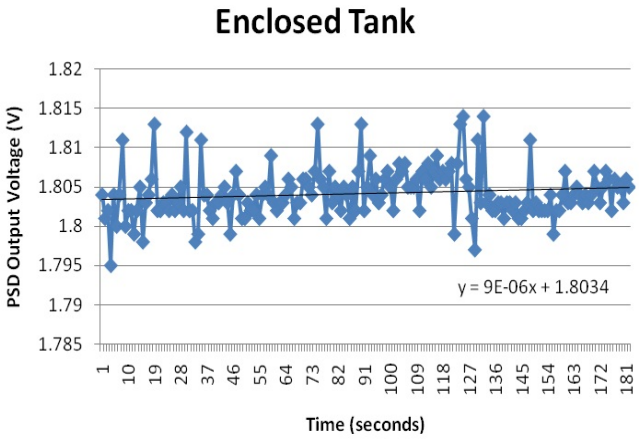

Fig. 6. Laser Drift vs. Time Through Enclosed

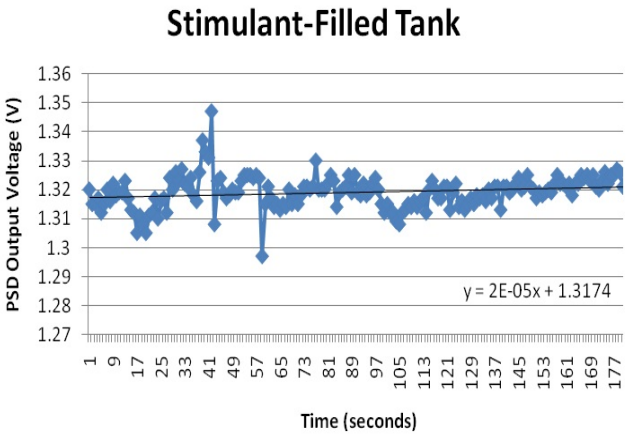

Fig. 7. Laser Drift vs. Time Through Stimulant Filled Tank

VII. Discussion

Our results characterize the pointing stability of the pigtailed laser under four distinct testing conditions. A general trend

TABLE II
LASER DRIFT OUTPUT IN MICROMETERS

	Open Air	Empty Tank	Enclosed Tank	Stimulant Tank
Ave. Drift	0.284	0..251	0..078	0..269
Std. Devation	3.163	1.075	1.090	2.642
Ave. Range	10.7	9.64	9.215	15.375
Std. Deviation	1.565	2.116	1.704	4.518

in our results was that as the driving current for the laser propagating in open air increased, the starting position or y-intercept would also increase. This means that increased input power to the laser caused unwanted effects of the beam drifitng upwards. This, however, was not the case with the other testing conditions as the obstructions in the path helped to isolate the beam from its environment and direct it better onto the surface of the PSD. The refractive changes of the glass tank cut back on the intensity of the beam while its plastic lid helped rememdy the effects of air flow in the lab, both of which produced a more steady initial starting point over all test runs.

The data in Tables I and II confirm that by enclosing the path of the beam, one can reduce the amount of drift exhibited by the laser onto the PSD. The average drift for open air propagation was .567 mV (.284 μm) which was significantly reduced to .157 mV (.078 μm) within the enclosed tank. Furthermore, the average range of drift was decreased from 21.4 mV (10.7 μm) in open air to 18.43 mV (9.215 μm).

Analysis of the position data for the tests with the stimulant-filled tank, however, showed that the beam deflected through the water more severely over the course of three minutes than it did in the other three testing environments. Although this may be a correct display of the laser's pointing stability through a fluid, it could have been caused by movement of the seemingly-stagnant water within the tank due to small thermal and mechanical vibrations that would not be detectable by the naked eye. A few small air pockets would also develop after placement of the plastic tray; these could have caused small amounts of movement within the liquid, which caused slight changes in the beam's path and were reflected in the recorded measurements.

VIII. SOURCES OF ERROR

We experienced sources of error in each facet of testing that caused us to adapt our testing methods that catered to each individual problem.

The laser stability still remained an issue in that the light that emerged from the tip of the coupled fiber diverged strongly before it reached the target microscope objective. This could be overcome by placing the laser directly in front of the lens such that they were nearly touching. This worked for initial testing purposes but ideally the fiber would have to touch the lens to eliminate all divergence, which could damage the laser and scratch the lens.

Ensuring the stability of all components is vital to the success of this design due to the sensitivity of the PSD, which can detect changes on the order of 10 nanometers. Mounting all parts of the setup rigidly became a challenge, as it was not possible to do so without sacrificing stability for use of available resources and machining capabilities. Testing of the laser required having the ability to adjust its position relative to other components, such as the lens and pinhole. The three-axis stage which the laser is mounted to introduces a large amount of instability into the overall system, which was compensated for by improving the mounts for the lens, pinhole, and PSD. Initial designs for the mounts proved faulty and inadequate, as they were made from thin pieces of metal and were not directly attachable to the optical surface; thus, newer, more solid blocks of aluminum were designed, to which the microscope objective and pinhole were attached. This system seemed more stable and less likely to have an effect on the fluctuation of laser beam position.

Power loss in our optic design proved to be an unexpected issue that affected the PSD measurements. Although high power coming out of the laser was not a strict requirement for the project, the optic devices used reduced the intensity of the laser so much that the beam incident upon the PSD was barely detectible. The microscope objective successfully reduced the beam's angle of divergence by a factor of three, but in doing so it also increased the size of it three-fold. This made the pinhole required for proper sizing of the beam through the tank which in turn reduced its brightness of the light coming out of the aperture. The tank itself also proved to be a source of power loss as the light would decrease in intensity as it underwent four refractive changes through the two sheets of glass. Combined together, this optical design often resulted in a SUM voltage that did not fall within the acceptable operating range.

The A-D converter used to transform the PSD voltages into a form that can be captured and analyzed by a computer introduced computational errors into our results. Because the converter has a finite bit-resolution there is a quantization error, Q = 20 / 2^{16} = .305 mV = .153 μm that is either added or subtracted to the actual value, resulting in an inaccurate readout from the VI. This makes it harder to analyze whether the beam was fluctuating greatly or if it was just an overshot value.

The environment that our tests were conducted in provided an uncontrollable source of error that affected many aspects of our results. When the laser was allowed to propagate in open air, convection air currents caused by the circulation of fluids due to small density changes as a result of small thermal fluctuations became present that would impede the beam causing it to drift further. Also, our operating table was a shared work space with other equipment whose contact with the table could cause slight vibrations felt by the mounts. Furthermore, the table itself was constructed with a steel top; the proximity of the assembly to the table prevented us from testing the effects due to the RF absorption. The ferrite core of the table would produce a magnetic field that in turn produces an electric field in the tank that can cause unwanted deflection of the beam.

IX. Conclusion

The preliminary tests we performed to characterize the pointing stability of the fiber-pigtailed laser may be built upon with future tests, under more controlled conditions, and with less potential sources of error. One improvement to the design explored through this project is to replace the A/D converter with one of a higher bit rate. This would result in more precise transmission of position data and therefore more accurate and conclusive results. Further research into appropriate collimating and focusing lenses is also necessary in order to achieve proper laser beam width without the use of multiple components which may skew the path of the beam slightly. Additionally, the effects of RF energy on the beam's deflection can be tested within an isolated and controlled environment, in order to determine if they are visible in the position data provided via the PSD. The ultimate goals for future advancement on this project are to maximize the stability of the overall system.

Acknowledgment

We would like to acknowledge the NSF, Dr. Christopher Davis, Dr. Vildana Hodzic, and graduate students John Rzasa, Navik Agrawal, and Ehren Hwang for their support and guidance with this project. We would also like to thank Joe Kselman for machining various parts of our assembly.

References

[1] M. Repacholi, A. Basten, V. Gebski, D. Noonan, J. Finnie, and A. Harris, "Lymphomas in E-Pim1 Transgenic Mice Exposed to Pulsed 900 MHz Electromagnetic Fields," *Radiation Research*, vol. 147, no. 5, pp. 631–640, 1997.

[2] J. Moulder, L. Erdreich, R. Malyapa, J. Merritt, W. Pickard, and Vijayalaxmi, "Cell Phones and Cancer: What Is the Evidence for a Connection?" *Radiation Research*, vol. 151, no. 5, pp. 513–531, 1999.

[3] "Questions and Answers about Biological Effects and Potential Hazards of Radiofrequency Electromagnetic Fields," Federal Communications Commission, Office of Engineering and Technology, Tech. Rep., August 1999.

[4] D. Seabury, "An Update on SAR Standards and the Basic Requirements for SAR Assessment," *Conformity*, pp. 1–7, 2005.

[5] J. Murphy and L. Aamodt, "Photothermal Spectroscopy Using Optical Beam Probing: Mirage Effect," *Journal of Applied Physics*, vol. 51, no. 9, pp. 4580–4583, September 1980.

[6] "Research and Regulatory Efforts on Mobile Phone Health Issues," United Sates General Accounting Office, Telecommunications, Tech. Rep., May 2001.

[7] C. Davis, Q. Balzano, V. Hodzic, and R. Gammon, "A Fast SAR Assessmet and Certification System for Wireless Device Certification," U.S. Patent 108 172-00 141, 2009.

[8] R. Paschotta. (2010, June) Single mode fibers. [Online]. Available: http://www.rp-photonics.com/single_mode_fibers.html